Time-resolved small-angle neutron scattering for characterization of molecular exchange in lipid nanoparticle therapeutics

Shayna L. Hilburg,*[a] Anna Sokolova,[b] Marina Cagnes,[b] and Lilo D. Pozzo*[a]

[a] *Department of Chemical Engineering, University of Washington, Seattle, WA, 98105, USA*

[b] *Australia Nuclear Science & Technology Organisation (ANSTO), Lucas Heights, NSW, 2234, Australia*

E-mail: shilburg@uw.edu and dpozzo@uw.edu

Phone: (206) 543-2250

Hypothesis: Nano-scale dynamics of self-assembled therapeutics play a large role in their biological function. However, assessment of such dynamics remains absent from conventional pharmaceutical characterization. We hypothesize that time-resolved small-angle neutron scattering (TR-SANS) can reveal their kinetic properties. For lipid nanoparticles (LNP), limited molecular motion is important for avoiding degradation prior to entering cells while, intracellularly, enhanced molecular motion is then vital for effective endosomal escape. We propose TR-SANS for quantifying molecular exchange in LNPs and, therefore, enabling optimization of opposing molecular behaviors of a pharmaceutical in two distinct environments.

Experiments: We use TR-SANS in combination with traditional SANS and small-angle x-ray scattering (SAXS) to experimentally quantify nano-scale dynamics and provided unprecedented insight to molecular behavior of LNPs.

Findings: LNPs have molecular exchange dynamics relevant to storage and delivery which can be captured using TR-SANS. Cholesterol exchanges on the time-scale of hours even at neutral pH. As pH drops below the effective pKa of the ionizable lipid, molecular exchange occurs faster. The results give insight into behavior enabling delivery and provide a quantifiable metric by which to compare formulations. Successful analysis of this multi-component system also expands the opportunities for using TR-SANS to characterize complex therapeutics.

Keywords: lipid nanoparticles; endosomal escape; SAXS; SANS; scattering; molecular exchange

Introduction

Lipid nanoparticle (LNP) therapeutics have revolutionized human health. The COVID-19 pandemic accelerated the pipeline for LNP-based vaccines, facilitating unprecedented rapid development and commercialization. Through this development and preceding it, many LNP complexities have been studied. However, the speed of commercialization necessitated bypassing some fundamental understanding, and there remains room for improvement in LNP manufacturing, safety, efficacy, and stability.[1] For LNP therapeutics to successfully deliver nucleic acids, components must traverse obstacles requiring a delicate balance of properties.[2] LNPs must maintain structural integrity in storage, delivery, and at physiological conditions to protect the cargo from degradation or exchange with biomolecules prior to entering the cell. However, these particles must then exhibit facile dissociation of components to undergo endosomal escape and deliver inside the cell.[3,4] Optimizing the trade-off between stability and deliverability could allow for more flexible storage requirements, such as reducing cold-chain storage needs, and improve efficacy which lowers required dosages, increasing safety and tolerance.

LNPs are comprised of five distinct molecular species: a cationic ionizable lipid, a zwitterionic "helper" lipid, a lipid with a poly(ethylene glycol) (PEG) head group, cholesterol, and nucleic acid cargo.[2] No covalent bonds connect the LNP components; rather, hydrophobic associations between lipid tails and cholesterol as well as electrostatic associations between nucleic acids and polar or charged lipid groups drive assembly. Therefore, molecules are free to move and, as in many self-assembled soft matter systems, the dynamic nature of LNP molecular associations are pivotal to their behavior. Toxicological concerns for LNPs result not only from the particle as a whole, but also on potential immunogenic responses from each individual component on its own, indicating that they each may interact with biological systems.[5] Dynamic behavior known to occur prior to endocytosis includes lipid mixing in initial formulation,[6] degradation from cargo exposure to nucleases, exchange with molecules (such as glycosaminoglycans) in the blood stream,[7] and shedding of the PEG-lipid layer impacting binding and protein adsorption.[8,9] After undergoing endocytosis, LNPs must then exchange lipids with the endosomal membrane to unpack cargo into the cytoplasm.[3] Successful endosomal escape is the limiting step in delivery, occurring for fewer than 10% of LNPs.[10,11] We therefore posit that understanding molecular dynamics of LNPs is key to unlocking maximal performance. However, current *in vitro* characterization focuses primarily on structural properties, relying on cell or animal studies to characterize performance metrics known to be impacted by dynamics. The molecular mobility in stable LNPs at equilibrium has not been considered to date, with dynamic evaluations having been limited to stability measures and assessments of aggregation, fusion, drug leakage, or chemical degradation.[12]

To learn how components move into and out of LNPs in different environments, we can first characterize how molecules exchange between multiple LNPs in solution. The complex interplay between hydrophobic and electrostatic driving forces to self-assembly makes such behavior difficult to predict. Experimental procedures for quantifying molecular dynamics *in situ* are necessary. Förster resonance energy transfer (FRET) assays can be effective for studying molecular exchange;[13] however, labeling requires bulky fluorophores which impact dynamics, especially of small molecules such as lipids and cholesterol. ^{1}H NMR can

characterize molecular mobility without requiring fluorophores, but is limited to short length- and time-scales.[14] We instead turn to small-angle scattering. Small-angle X-ray and neutron scattering (SAXS and SANS) are effective for characterizing LNP structures from Angstroms to hundreds of nanometers.[1,15,16] SANS is particularly powerful for studying biomacromolecules, as contrast can be changed using selective deuteration to enable isolated visualization of specific components, and has been used with great effect characterizing LNP structure.[17,18] Such isotopic labeling has minimal effect on molecular behavior, though isotopic effects do exist. For example, aggregation driven by hydrophobic interactions is slightly strengthened in D_2O (heavy water) compared to H_2O due to its stronger hydrogen-bonding network and the reduction of van der Waals interactions.[19] While these effects must be noted, they are minimal compared to changes imparted by fluorescent tags.

In recent years, the variable of time has been incorporated into SANS to observe phenomena *in situ*, enabled by higher flux beam lines that can make faster measurements and creative in-beam apparatuses.[20,21] By coupling selective deuteration with time-resolution, molecular exchange between protonated and deuterated populations of molecules can be observed. Our group, and others, have used such time-resolved contrast variation SANS (TR-SANS) to capture molecular exchange in self-assembled soft matter.[22–25] TR-SANS can capture changes on the order of seconds (if strongly scattering) to days. It requires at least one deuterated component and a selected solvent in which the linear combination of scattering from deuterated and protonated populations is different from the scattering of a population created with pre-mixed deuterated and protonated molecules. This complexity has limited prior TR-SANS experiments to structures with one or two components. LNPs, on the other hand, typically contain five components. Therefore, using TR-SANS for LNPs introduced uncertainty to an already complex technique.

An ideal TR-SANS molecular exchange experiment contrast matches every component except for the one whose exchange will be studied. Assay populations then contain either entirely protonated or entirely deuterated versions of this component of interest, such that measured scattering signal is due only to the exchanging molecule. Upon mixing these populations, molecules exchange in solution between all structures, eventually reaching a contrast-match condition themselves such that the structure no longer scatters. However, experiments are non-ideal, and an unfortunate limitation of contrast variation techniques is that deuterated materials are difficult to obtain. While simple deuterated molecules are commercially available, more complex molecules such as state-of-the-art and proprietary lipids require advanced synthetic techniques and are often obtained through collaboration with industrial partners or one of few government agencies which specialize in this work. TR-SANS provides incomparable data that will greatly enhance the understanding of biomaterials, such as LNPs. To maximize the impact of TR-SANS, access to deuterated molecules must be enhanced. That withstanding, in this work, we use TR-SANS to characterize LNP molecular exchange that has implications for drug accessibility and efficacy with only partial contrast-matching.

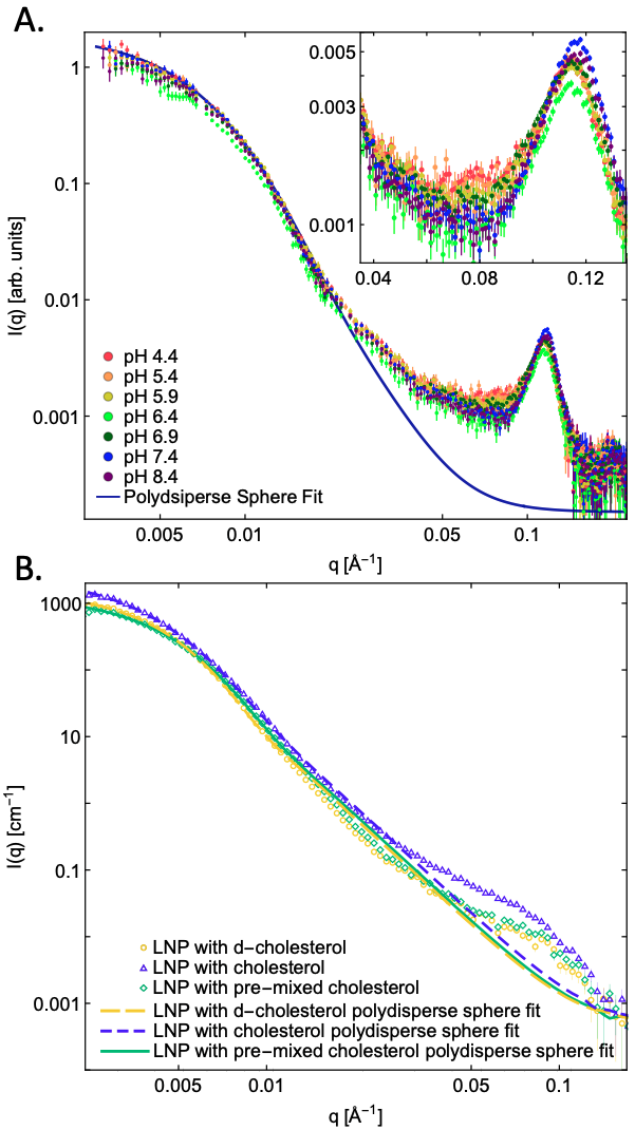

Fig. 1 (A) SAXS measurements of LNPs in PBS as a function of pH with inset showing a larger zoom and linear q axis for the feature at $q \approx 0.1$Å^{-1} and (B) SANS measurements of LNPs in d-PBS at pH 7.4 of three synthesized populations: LNPs with 100% d-cholesterol, LNPs with 100% cholesterol, and LNPs with 50:50 d-cholesterol and cholesterol premixed.

We obtained deuterated cholesterol (d-cholesterol) through Australia's National Deuteration Facility. As cholesterol makes up a significant portion of volume in current LNP formulations, we anticipated that there would be sufficient scattering length density differences between LNPs synthesized with d-cholesterol versus cholesterol to enable molecular exchange experiments without the need to obtain fully deuterated versions of all other components. The other LNP components are either minimal volumetric contributions or more difficult to obtain deuterated. Although exchange of all components has relevance to LNP function, we propose that cholesterol exchange can be used as a signal for molecular exchange overall. Cholesterol is hydrophobic, and therefore would not be expected to pass the hydrophilic LNP surface and through solution to other LNPs independently.

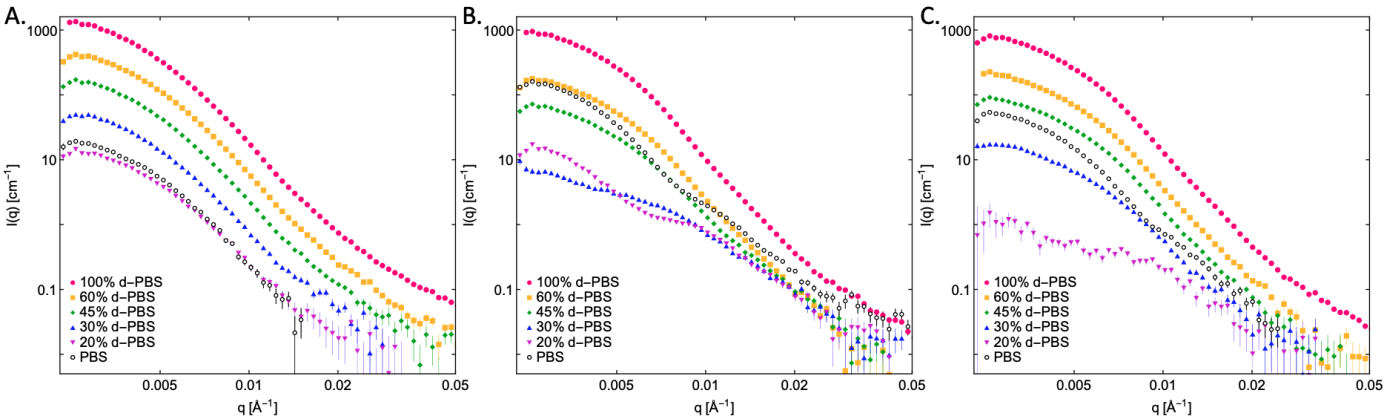

Fig. 2 SANS scattering curves for LNPs at pH 7.4 in varied d-PBS:PBS ratios made containing (A) 100% cholesterol, (B) 100% d-cholesterol, and (C) a 50:50 pre-mixed combination of d-cholesterol and cholesterol.

The solubility of cholesterol in water is approximately 2.5×10^{-5} mg/mL and even decreases slightly with the addition of salt.[26,27] Therefore, the cholesterol is likely transported through the buffer with amphiphilic lipids. Our results can therefore suggest a lower bound on molecular exchange for other LNP components. Herein, we share the first quantification of inter-particle molecular exchange of cholesterol exchange in LNPs using TR-SANS. While TR-SANS has been used to characterize molecular exchange dynamics of self-assembled soft matter in the past, LNPs are more complex multi-component systems than previously studied for which it would be challenging and reductive to simplify their compositions. We also probe pH-dependence of the LNP molecular exchange. Experimental literature has examined internal structure at different pHs, suggesting decreased lipid ordering in the endosome,[28,29] and simulations have seen pH-dependent lipid dynamics in simplified leaflet systems.[28] Molecular exchange of LNP components would optimally be pH-dependent: minimized during storage and delivery prior to entering cells, and maximized intracellularly. Therefore, our results provide therapeutically-relevant insight to LNP behavior.

Materials and Methods

LNPs were synthesized following existing literature recipes.[18] LNPs comprised 1.5 mole % 1,2-Dimyristoyl-rac-glycero-3-methoxyPEG-2000 (DMG-PEG(2000)) (Cayman Chemical Company, Michigan, USA), 10 mole % 1,2-Distearoyl-sn-glycero-3-PC (DSPC) (Cayman Chemical Company, Michigan, USA), 50 mole % 4-(dimethylamino)-butanoic acid, (10Z,13Z)-1-(9Z,12Z)-9,12-octadecadien-1-yl-10,13-nonadecadien-1-yl ester (DLin-MC3-DMA or MC3) (Cayman Chemical Company, Michigan, USA), 38.5 mole % protonated cholesterol (cholesterol) (Cayman Chemical Company, Michigan, USA) and/or deuterated cholesterol (d-cholesterol) (cholesterol-d_{45} (C_27HD_45O) from ANSTO Australian National Deuteration Facility with 79 ± 2 %D by mass spectrometry prepared according to published methods[30]), and a 60-nucleobase single stranded DNA (ssDNA) (Integrated DNA Technologies, Iowa, USA) sequence at an amine to phosphate ratio (N:P) of 3. Use of ssDNA provides polyanionic nucleic acid cargo without the cost and experimental difficulty of using RNA. Physicochemical properties governing molecular exchange are expected to trend similarly. To perform solvent injection LNP synthesis, lipids were combined in solution in ethanol prior to being rapidly pipette into ssDNA in acidic citrate buffer. A buffer exchange process was then used to filter and replace solvent with phosphate buffered saline (PBS) or deuterated PBS (d-PBS) of varied pH. As the effective pKa of MC3 within LNPs is 6.4,[2] pH conditions were selected around this value. Details of these solutions and exchange processes are provided in Supplementary Information 1.1. SAXS was performed on a Xenocs Xeuss 3.0 (Grenoble, France) at room temperature (approximately 20°C) at multiple sample-to-detector distances detailed in Supplementary Information. SANS was performed on the Bilby instrument at the Australian Centre for Neutron Scattering at 25°C.[31,32] All data have had solvent contributions subtracted. Additional SAXS and SANS details are available in Supplementary Information 1.3 and 1.4.

Results & Discussion

SAXS data collected for a wide range of pH values (4.4 through 8.4) shows that low q data remains relatively unchanged, indicating consistency of macroscale features (Figure 1A). Low q data is fit with polydisperse spheres with 15 to 16 nm radii (fit for pH 7.4 data shown in Figure 1A, additional fits and parameters in Supplementary Information 1.3). Dilute sample conditions were selected to avoid the impact of structure factor effects on the scattering. At the low concentration used, the LNPs are far apart from one another and, therefore, interparticle correlations are negligible such that only the form factor is dominant in the scattering. Spherical size increases slightly with pH for most conditions, though with the radius changes spanning only a range of 9 , the size and size distribution can be said to remain similar for LNPs as pH changes despite charge state differences of internal components. Hydrophobicity, therefore, is likely the dominant factor dictating surface area to volume ratios. Low q feature shapes seen in SAXS are also visible in SANS data from LNPs in 100% d-PBS at pH 7.4 (Figure 1B). The low q LNP data are again fit by polydisperse spheres, though radii of 39, 32, and 34 nm for the d-cholesterol, cholesterol, and pre-mixed cholesterol popu-

lations, respectively, are found (details in Supplementary Information 1.4). The larger radius from SANS compared to SAXS is likely due to the PEG corona, as the PEG-lipid does not have contrast in PBS to X-rays but has significant contrast to neutrons in d-PBS (scattering length densities, or SLDs, for all components found in Supplementary Information 2). Additionally, due to experimental limitations, the LNP syntheses for the SAXS and SANS experiments were executed at different times with slightly different protocols, perhaps creating size differences.

A sharp peak at $q \approx 0.1 \text{Å}^{-1}$ is apparent in the SAXS data (Figure 1A). The feature is less sharp in SANS results, consistent with literature and likely due to contrast differences between methods. The peak corresponds to lipid ordering within the nanoparticles.[16,29] There is some excess scattering above the sphere fit in SANS data which may correspond to the same structural features. However, lipid contrast varies between the two techniques, as confirmed by the scattering length density (SLD) values for each component in Supplementary Information 1.2. Contrast between head groups, lipids, and nucleic acids provides the greatest signal in SAXS whereas contrast between solvent and all lipid structures provides the greatest signal in SANS. Therefore, the internal lipid packing produces the more prominent feature seen in the inset of Figure 1A. The feature broadens and shifts slightly as the pH drops, which existing literature correlates to a change in ordering.[28,29] The precise nature of the phase changes within LNPs are formulation-dependent, though there is agreement that a pH-driven structural evolution impacts lipid ordering.[16,28,29,33] While research has shown the pronounced effect pH can have on LNP internal structure as MC3 changes charge state,[29,34] experimental work has often used unfiltered and ethanol-containing solvent resulting from synthesis as the acidic condition, which is less representative of endosomal environments than PBS.[29] Our results here indicate that the trends hold true as a function of pH in PBS, rather than as an effect of filtering and buffer exchange.

The SANS data in Figure 1B depicts scattering for each LNP population needed for the molecular exchange experiment: LNPs with 100% d-cholesterol, LNPs with 100% cholesterol, and LNPs with 50:50 d-cholesterol and cholesterol pre-mixed prior to assembly. In pure d-PBS, the 3 populations are fit with similar radii, indicating relative consistency between the structures despite differences in cholesterol protonation. Each population was then examined at varied d-PBS:PBS ratios (Figures 2A, B, and C) to find a suitable solvent condition. Upon mixing for a kinetics assay, the d-cholesterol and cholesterol populations will scatter independently in dilute solution and manifest as the arithmetic mean of their independent scattering curves. As molecular exchange progresses, scattering will shift towards that of the pre-mixed population. The pre-mixed population is equivalent to LNPs in which cholesterol has fully exchanged, having 50% d-cholesterol and 50% cholesterol fully mixed throughout the structure. In Figure 2, the shapes of the curves clearly differ between d-cholesterol, cholesterol, and pre-mixed cholesterol populations as the solvent deuteration changes. These differences are most noticeable in the mid q range, around q 0.004–0.030 Å^{-1}. At q greater than 0.02 Å^{-1}, noise due to incoherent scattering dominates low d-PBS conditions. Therefore, the q range from minimum to 0.020 Å^{-1} was selected to evaluate the point of minimum intensity (PMI) for each population. The integral of intensity over this range was calculated for each condition. Second order polynomials were

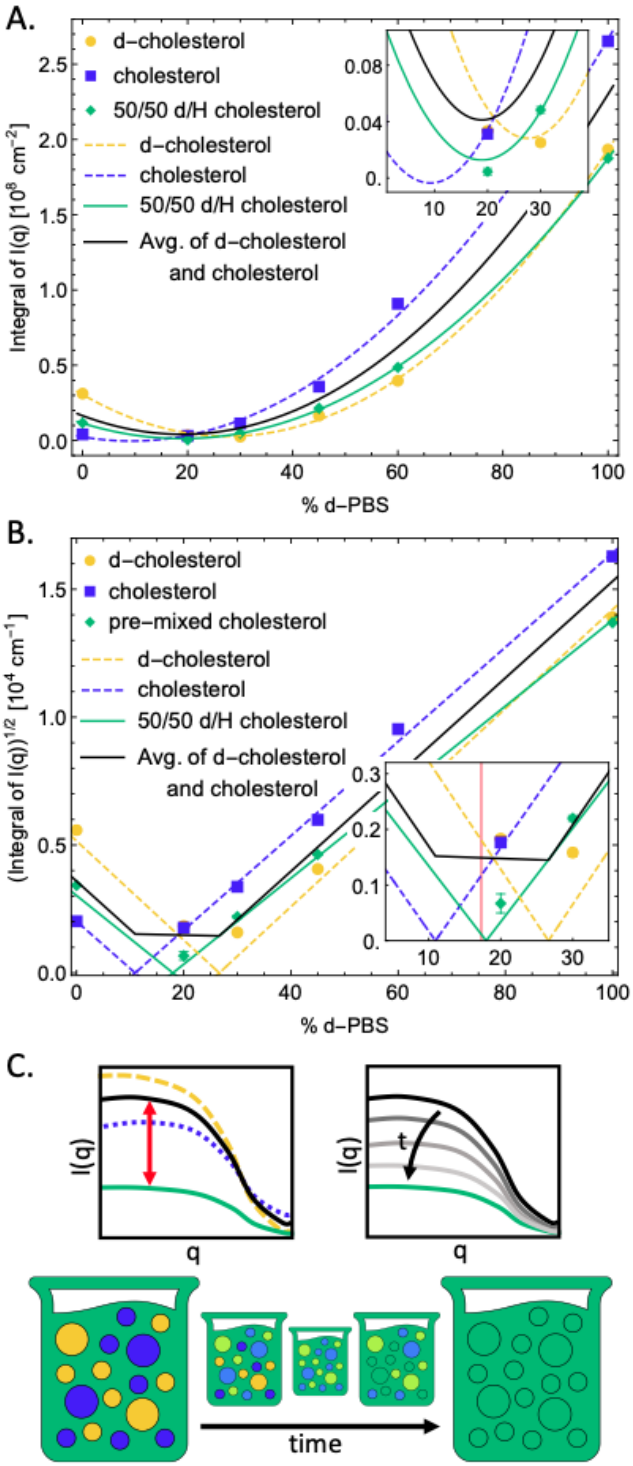

Fig. 3 Analysis for determination of experimental solvent contrast condition through (A) scattering intensity integral data as a function of percent deuterated solvent with second order polynomial fits as well as (B) square-root of scattering intensity integral data as a function of percent deuterated solvent with first order fits, as well as (C) an experimental schematic depicting the expected molecular exchange assay.

then fit to these results, as shown in Figure 3A. For simpler analysis in units of intensity, the square root of these values was then calculated and assigned charge based on positioning relative to the polynomial fits. This data was then fit with the absolute value of a linear equation, shown for each population in Figure 3B. The ideal solvent for the molecular exchange assays maximizes the difference between pre-mixed cholesterol and the arithmetic mean of the d-cholesterol and cholesterol populations (representing what would be present in solution immediately upon mixing). The selected experimental condition was 17.3% D_2O, marked with a vertical red line in Figure 3B. Conceptually, Figure 3C shows in red how this difference should translate to scattering curves and carry through to time-resolved experiments. Finding a sufficient contrast point is not trivial nor guaranteed. Systems could have contrast points greater than 100% deuterated solvent or less than 0% protonated solvent or the difference in intensity could be less than measurement noise. For example, deuterated DSPC lipid is impossible to match with aqueous solvents, as its scattering length density is greater than that of D_2O.[35] Therefore, finding this solvent condition is, itself, a major achievement for LNP characterization.

Upon determining the contrast condition, kinetics samples were prepared by mixing 50% volume each of d-cholesterol and cholesterol LNP populations and then collecting scattering profiles over time. Curves denoted with the average time after mixing (scattering performed for 1 hour, from 30 minutes before through 30 minutes after the labeled time) are shown in Figure 4A for the sample at pH 7.4. Sample scattering decreases from its initial value towards the scattering of a pre-mixed population (taken as reference representing complete molecular exchange) as time evolves, indicating that cholesterol is exchanging between LNPs of each population in the solution. A comparison of pure d-cholesterol and cholesterol LNP populations before and after the kinetics confirmed that time evolution is due to molecular exchange rather than structural change (Supplementary Information 2).

To quantify molecular exchange from the scattering profiles, intensity was integrated from $q = 0.003$–0.010 Å^{-1} for each profile and depicted in Figure 5A. This integration range was narrower than the range used for solvent contrast selection due to increased noise at the shorter kinetics run time. The integrated scattering intensities were then converted to a relaxation function, $R(t)$, per Equation 1,[23] where $I(t)$ is the integrated scattering intensity at time t. I_∞, the integrated scattering intensity after infinite time, was set equal to that of the pre-mixed cholesterol population. Initial integrated scattering intensity, I_0, was set equal to the first kinetic sample time point ($t = 31$ min). $R(t)$ of 1 corresponds to the initial condition, while $R(t)$ of 0 corresponds to LNPs which have fully exchanged cholesterol and contain 50% of each type.

$$R(t) = \left(\frac{I(t) - I_\infty}{I_0 - I_\infty}\right)^{1/2} \quad (1)$$

$$R(t) = e^{-kt} \quad (2)$$

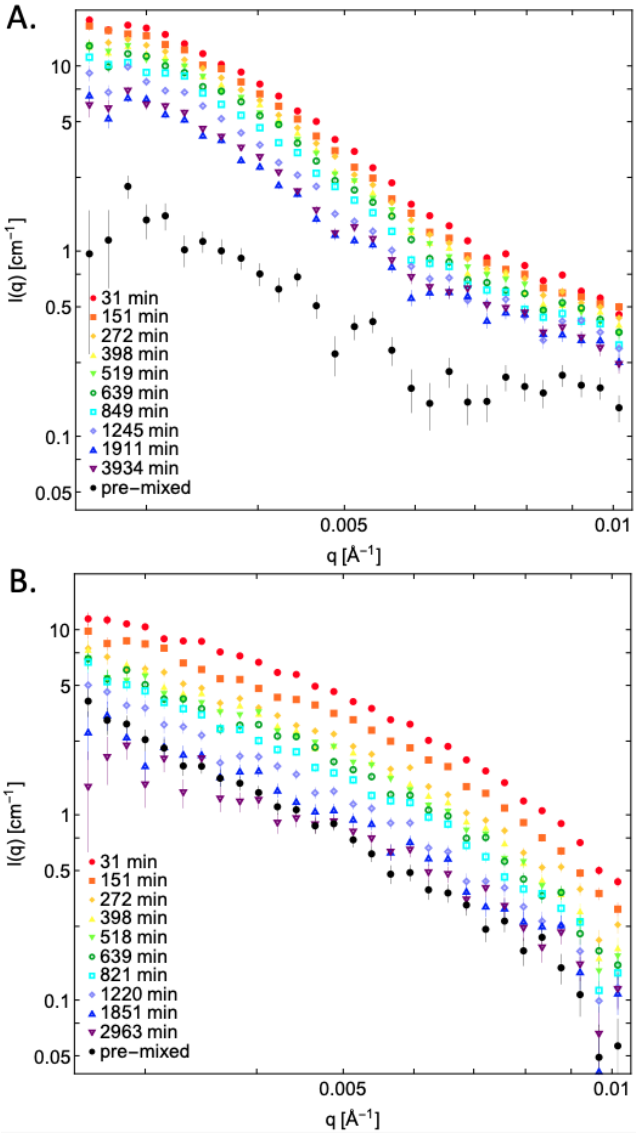

Fig. 4 Molecular exchange of cholesterol in LNPs. SANS profiles during kinetics assay over time at (A) pH 7.4 and (B) pH 4.4 including pre-mixed cholesterol reference profiles in black dashed lines.

$$R(t) = (1-c)e^{-kt} + c \quad (3)$$

The resulting $R(t)$ data in Figure 5B shows a steady decay until the final point, $t = 3934$ min, where the $R(t)$ value increases slightly rather than continuing to decrease. The general downward trend seen in $R(t)$ as t progresses from the initial condition to almost 2000 min (approximately 32 hours), confirms our hypothesis that molecular exchange of cholesterol can be observed through TR-SANS and that, despite being referred to as "nanoparticles", LNPs are in fact mobile assemblies between which molecules can and will dynamically exchange. Furthermore, the $t = 3934$ min point introduces an interesting possibility that had not been anticipated. Although this is only a single data point, and should be replicated to confirm related hypotheses, the plateau before reaching an $R(t)$ of 0 indicates that molecular exchange is no longer progressing on the experimentally available

time frame. By comparing to the pre-mixed population, it is clear that exchange of cholesterol between LNPs is somehow limited to only a portion of the total cholesterol while another portion stays isotopically separated. Rather than continuing towards $R(t) = 0$, a subset of the cholesterol remains within individual LNPs and is not exchanged amongst them. We hypothesize that in the pH 7.4 LNP structure, the initial cholesterol exchange only occurs for an accessible subset of molecules closer to the liquid interface. The cholesterol deeper within the core of the LNP would be less mobile than cholesterol closer to the corona, and its inter-particle exchange occurs on too long a time-scale to capture. Therefore, while the outer shells continue exchanging cholesterol, the cores maintain their initial d-cholesterol or cholesterol populations, as depicted schematically in the top of Figure 6. When fitting an exponential decay function to the relaxation from $R(t) = 1$ to $R(t) = 0$ (detailed in Supplementary Information 3), we therefore excluded $t = 3934$ min data. Using the remaining data, an exponential decay model bound from 0 to 1, Equation 2, was fit to pH 7.4 data and a relaxation rate of $k = 3.5 \times 10^{-4}$ min^{-1} was determined. In reality, there may be two relaxation rates at pH 7.4, with the exchange of the internal sub-population of cholesterol having a much lower exchange rate, and making its observation outside the experimental time frame. Accounting for the plateau value requires the addition of a constant, c, per Equation 3. Note that Equation 3 collapses to Equation 2 when $c = 0$. This constant represents the plateau value and fitting to the equation provides a rate for the first part of exchange of $k = 10.4 \times 10^{-4}$ min^{-1}. With a plateau value fit of 0.53, this rate is characteristic for the first half of the cholesterol exchange, while the remaining half is not exchanged within the experimental time frame at pH 7.4.

Now that TR-SANS has been demonstrated on LNP therapeutics, more extensive investigations are warranted, and could provide insight into the observed behavior. In the current experiment, our kinetic scattering contribution are from the exchange of cholesterol isotopes, but the pre-mixed sample equivalent to t_∞ acts as a baseline to all measurements and includes scattering contribution from the other 4 components. Alternatively, a fully contrast-matched system–LNPs incorporating deuterated populations of DMG-PEG(2000), DSPC, MC3, and nucleic acid cargo in addition to the d-cholesterol used in this work–could be created such that the scattering observed at t_∞ would be minimized. This would increase the difference between initial and final conditions for the kinetics assay and, therefore, improve resolution. Secondly, deuterated populations of the other components would enable molecular exchange rate assays for all components and an ability to compare. Given the different molecular exchange rates for heterogeneous lipid membrane constituents, each LNP component also likely has its own chemically-dependent rate that can be studied. Additionally, the nuanced results indicating a stagnant sub-population of molecules at pH 7.4 prompts us to consider future structural analyses. Detailed static analysis of LNP samples allowed to exchange for several days, akin to the final time-points in this work, could expose information about the 53% of cholesterol which remains isotopically segregated at pH 7.4 in an intermediate structure, distinct from the infinite mixing controls, which illuminates the mechanism for partial exchange. Analyzing contrast variation results from selectively deuterated samples through methods (such as a Stuhrmann analysis[36]) would provide detailed results similar to Sebastiani et al.'s LNP structural studies for this intermediate. Our hypothesized mechanism, Figure 6, envisions a core-shell type morphology with an outer region which would fully exchange while an inner core remains isotopically homogenous. This mechanism would appear as concentric spheres. Contrastingly, an alternate mechanism could see some uniformly distributed sub-population of cholesterol remaining unexchanged, which would manifest as a sphere equivalent in radius to the initial ($t = 0$) scattering fit but with different contrast. Therefore, continued experiments on this system could illuminate whether the core-shell type localization of cholesterol is in fact what determines its propensity to exchange in the first rapid relaxation period. The mode in which molecules exchange can also be further studied by measuring the exchange rate k as a function of LNP concentration. The exchange rate would increase as concentration increases if driven by collisions, but decrease if relying on component solubility as the solubility limit would be reached sooner. Given the low solubility of cholesterol in PBS,[26,27] we hypothesize the cholesterol exchange does not rely on cholesterol dissolution, and will be driven, at least in part, by LNP collisions. Another potential mechanism involves cholesterol molecules being carried along with other components and these clusters of molecules may be exchanged via dissolution and resorption, where the cholesterol can be sheltered by more soluble amphiphilic lipids. If dissolution and resorption alongside other components drives a portion of cholesterol exchange, the rate found within the present study can act as lower bound on lipid exchange and be considered a proxy for exchange of other LNP components. Ultimately, a combination of mechanisms could be at play. Even without the proposed next experiments, considering only the overall relaxation rate and the exchange quantified within the time frame of the current work, our results still demonstrate that even the most hydrophobic LNP components can exchange within hours at pH 7.4, indicating therapeutically relevant dynamics.

The impact of pH-driven changes on molecular exchange was then examined using the same kinetic assay method at pH 4.4, below the effective pKa of the ionizable lipid. SAXS results showed that LNP structure changed only subtly upon transitioning from above pH 6.4 to below. However, kinetics results show a drastic and obvious change. Qualitatively, Figure 4B shows a more rapid decrease from the initial scattering ($t = 31$ min) such that within the same time frame as the pH 7.4 sample, the acidic sample reaches the pre-mixed LNP scattering and indicates complete cholesterol population exchange. Figures 5A and B show that quantitatively, the full exchange occurs at almost 3 times the rate at pH 4.4 as pH 7.4, having a relaxation rate of $k = 9.6 \times 10^{-4}$ min^{-1} when fit to Equation 2. The exchange rate at pH 4.4 is similar to the $k = 10.4 \times 10^{-4}$ min^{-1} fit to Equation 3 for the first half of cholesterol exchange at pH 7.4. However, the plateau value at pH 4.4 is 0 (indicating that the data captured within the experiment trends towards $R(t) = 0$ at infinite time), and the full exchange of cholesterol populations therefore occurs much more rapidly than at pH 7.4. Per the schematics in Figure 6, we hy-

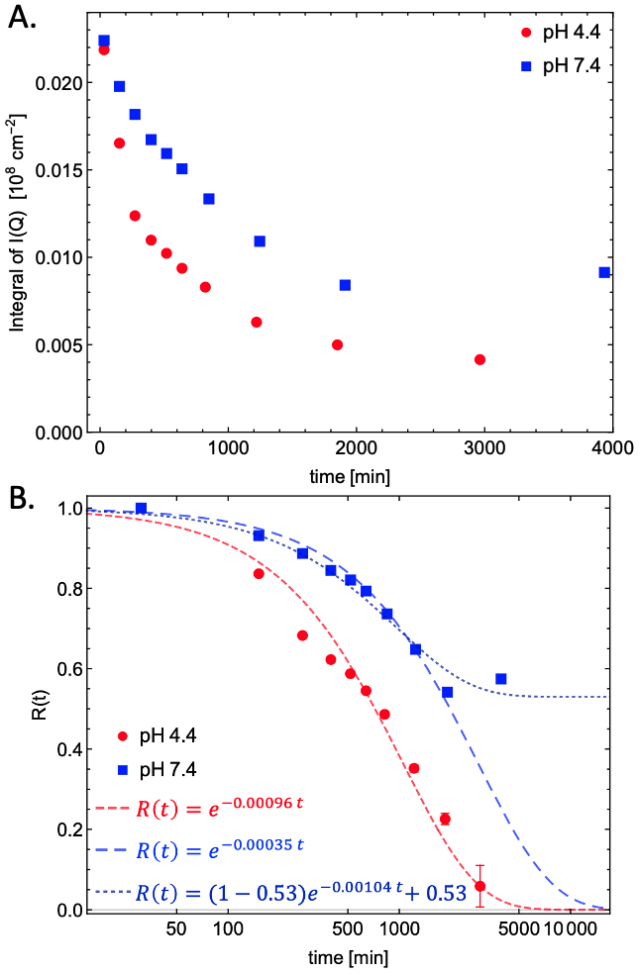

Fig. 5 The (A) integrated scattering intensity over time for each molecular exchange condition as well as the correlating (B) relaxation function with exponential decay curve fits. Where error bars are not visible, they are smaller than the point size.

pothesize that internal structural changes enable all cholesterol throughout the LNPs to exchange in the acidic environment. The change in lipid ordering in acidic solution suggested from SAXS analysis and phase changes documented for bulk lipid structures, which pack with less curvature in acidic conditions,[16] could reduce the enthalpic penalty to molecular motion, create easier access to the solution, and contribute to the increased rate of exchange at pH 4.4. Even at more than double the rate of pH 7.4, the pH 4.4 sample still shows cholesterol exchange in LNPs to be an order of magnitude slower than the exchange of oil in surfactant-stabilized emulsions previously characterized by our group, and multiple orders of magnitude slower than the chain exchange observed in block and random copolymer micelles by others.[22,23,37,38] The exchange rates for cholesterol we calculated are, on the other hand, actually comparable to those for the exchange of molecules in another lipid-based system: the interbilayer molecular exchange of phospholipids.[39] Although Gerelli et al. characterized interbilayer phospholipid exchange at elevated temperatures (ranging between between 0.003 and 0.03 min^{-1} at 48 to 68°C), an extrapolation of their data to lower temperature provides an interbilayer exchange rate of approximately 4×10^{-4} min^{-1} and 7×10^{-4} min^{-1} for 5 mg/mL and 1 mg/mL samples, respectively, at 25°C. The lipid layers within the solid supported bilayer system examined were necessarily in close proximity, whereas the LNPs in the current investigation are free in solution. Additionally, in the lipid bilayer system, it is known that cholesterol flip-flops between layers orders of magnitude faster than phospholipids (on the order of milliseconds versus hours),[40] as it does not require exposure of hydrophilic moieties to the hydrophobic tails inside the bilayer as phosophlipid exchange does. LNPs differ in many ways from lipid bilayers, but the similarity in rate certainly raises interest in the similarity between disrupting self-assembled constructs of amphiphilic molecules driven by hydrophobic effects. Despite the relatively slow inter-LNP exchange rate we found for cholesterol, pharmaceutical storage and circulation are highly sensitive to molecular dynamics and the quantified values leave room for improvement. Formulation design and optimization could be useful in decelerating exchange at neutral conditions and accelerating intracellular exchange.

Conclusions

Our results show that TR-SANS provides an unprecedented view of molecular dynamics in LNPs without structural simplification. Further investigation will be required to understand how formulations can maximize the difference between dynamics in neutral versus acidic environments, as well as how exchange of other components correlate to cholesterol. This work provides a framework with which dynamics of additional components, alternate formulations, and other solution environments can be probed to ultimately enable optimization for more effective therapeutics. We have demonstrated a valuable tool for characterizing dynamics of self-assembled LNP systems. Despite the complexity and expense of TR-SANS, the technique provides unprecedented insight into environmentally-dependent molecular exchange between LNP therapeutics. The characterized exchange demonstrates significant exchange of LNP components within hours, indicating molecular mobility that can impact both storage and delivery. Even at neutral conditions, LNPs are constantly exchanging molecules rather than existing as a static structure akin to a nanoparticle formed through covalent bonds. Reducing this dynamic behavior could avoid degradation and greatly enhance storage stability. In considering cellular delivery, the time-scale of exchange quantified is longer. However, the mechanisms of endosomal escape would require the same type of lipid motion and relate directly to the quantified properties. A comparison of neutral and acidic conditions showed an exchange rate almost three times faster in lower pH, bolstering a molecular rationale for escape from the acidic endosome informed by prior static studies of pH-driven structural changes.[16,33,41] Through *in situ* dynamics studies, we were able to quantify the implication of such structural changes on molecular behavior. Coupling our work with recent in-depth structural analyses can inform chemical modifications to improve the dynamic trade-offs in different stages of delivery.[15,18] We have also paved the way for further use of TR-SANS on LNPs, enabling quantifiable comparison of

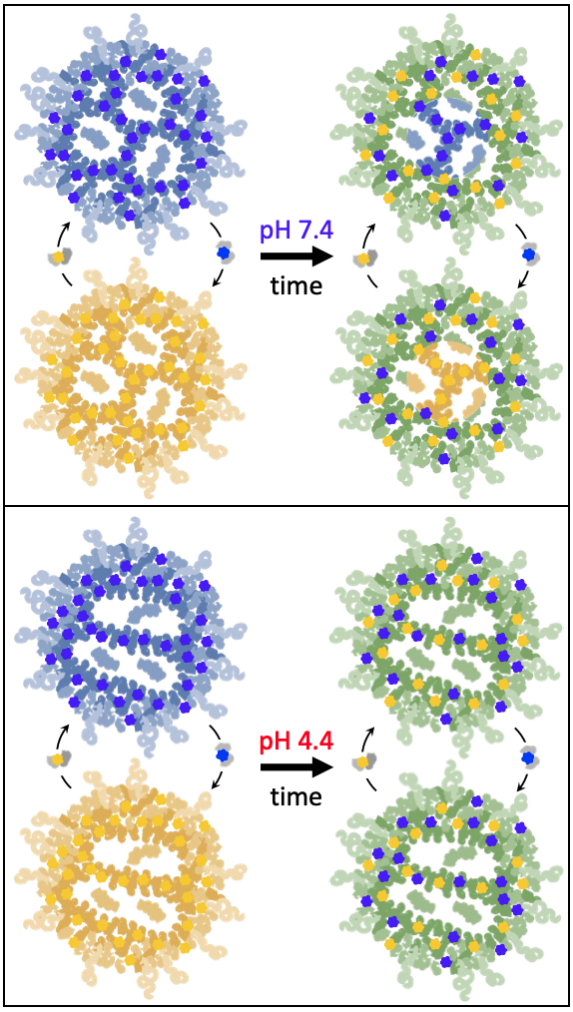

Fig. 6 Schematic shows hypothesized cholesterol exchange at each pH, using LNP depictions structurally informed by Cárdenas et al., Philipp et al., and Sebastiani et al..[1,16,18] Regions hypothesized to contain only protonated cholesterol are depicted in blue, regions hypothesized to contain only deuterated cholesterol are depicted in yellow, and regions hypothesized to contain an equal mix of the two are depicted in green.

formulations. Eventually, the difference between exchange before and after endocytosis can be maximized to optimize both stability and deliverability. Furthermore, our results also demonstrate the capability of executing TR-SANS on self-assembled systems with greater complexity than previously studied.[22–25] Finally, the use of d-cholesterol which enabled this work provides motivation to seek deuterated versions of other components to study their exchange amongst LNPs and with biological serum and membranes. Deuterated materials are often sourced from one of few government facilities throughout the world, or procured through industrial collaboration.[18] This hurdle could limit the potential of TR-SANS for complex biomaterials. Therefore, partnerships with pharmaceutical companies and continued support for deuteration facilities will be vital to maximizing impact and ultimately optimizing LNPs and other molecular constructs. With such materials and further experiments, TR-SANS studies may eventually provide prescriptive dynamic insights to control the function of self-assembled therapeutics.

Acknowledgements

We acknowledge the support of the Australian Centre for Neutron Scattering, ANSTO and the Australian Government through the National Collaborative Research Infrastructure Strategy, in supporting this work via Neutron & Deuteration Proposal 15396. The National Deuteration Facility is partly funded by the National Collaborative Research Infrastructure Strategy (NCRIS) – an Australian Government initiative. Thanks to Sage Scheiwiller and Karen Li for assistance during experimentation. We acknowledge the use of SAXS facilities and instrumentation supported by the U.S. National Science Foundation through the Major Research Instrumentation (MRI) program (DMR-2116265) and by the UW Molecular Engineering Materials Center, a Materials Research Science and Engineering Center (Grant No. DMR-1719797). This work benefited from the use of the SasView application,[42] originally developed under NSF award DMR-0520547. SasView contains code developed with funding from the European Union's Horizon 2020 research and innovation programme under the SINE2020 project, grant agreement No 654000. This material is based upon work supported by the National Science Foundation under Grant EEC-2127509 to the American Society for Engineering Education.

References

1 M. Cárdenas, R. A. Campbell, M. Yanez Arteta, M. J. Lawrence, F. Sebastiani, Review of structural design guiding the development of lipid nanoparticles for nucleic acid delivery, Current Opinion in Colloid and Interface Science 66 (2023) 101705. doi:10.1016/j.cocis.2023.101705.
URL https://doi.org/10.1016/j.cocis.2023.101705

2 M. D. Buschmann, M. J. Carrasco, S. Alishetty, M. Paige, M. G. Alameh, D. Weissman, Nanomaterial Delivery Systems for mRNA Vaccines, Vaccines 9 (1) (2021) 65. doi:10.3390/vaccines9010065.
URL https://www.mdpi.com/2076-393X/9/1/65

3 B. M. Bruininks, P. C. Souza, H. Ingolfsson, S. J. Marrink, A molecular view on the escape of lipoplexed DNA from the endosome, eLife 9 (2020) 1–16. doi:10.7554/eLife.52012.
URL https://elifesciences.org/articles/52012

4 A. Yen, Y. Cheng, M. Sylvestre, H. H. Gustafson, S. Puri, S. H. Pun, Serum Nuclease Susceptibility of mRNA Cargo in Condensed Polyplexes, Molecular Pharmaceutics 15 (6) (2018) 2268–2276. doi:10.1021/acs.molpharmaceut.8b00134.
URL https://pubs.acs.org/doi/10.1021/acs.molpharmaceut.8b00134

5 D. Bitounis, E. Jacquinet, M. A. Rogers, M. M. Amiji, Strategies to reduce the risks of mRNA drug and vaccine toxicity, Nature Reviews Drug Discovery (2024). doi:10.1038/s41573-023-00859-3.

6 G. Caracciolo, D. Pozzi, H. Amenitsch, R. Caminiti, Multicomponent Cationic Lipid-DNA Complex Formation: Role of Lipid Mixing, Langmuir 21 (25) (2005) 11582–11587. doi:10.1021/la052077c.

URL https://pubs.acs.org/doi/10.1021/la052077c

7 S. Osawa, K. Osada, S. Hiki, A. Dirisala, T. Ishii, K. Kataoka, Polyplex Micelles with Double-Protective Compartments of Hydrophilic Shell and Thermoswitchable Palisade of Poly(oxazoline)-Based Block Copolymers for Promoted Gene Transfection, Biomacromolecules 17 (1) (2016) 354–361. doi:10.1021/acs.biomac.5b01456.
URL https://pubs.acs.org/doi/10.1021/acs.biomac.5b01456

8 B. L. Mui, Y. K. Tam, M. Jayaraman, S. M. Ansell, X. Du, Y. Y. C. Tam, P. J. Lin, S. Chen, J. K. Narayanannair, K. G. Rajeev, M. Manoharan, A. Akinc, M. A. Maier, P. Cullis, T. D. Madden, M. J. Hope, Influence of Polyethylene Glycol Lipid Desorption Rates on Pharmacokinetics and Pharmacodynamics of siRNA Lipid Nanoparticles, Molecular Therapy - Nucleic Acids 2 (12) (2013) e139. doi:10.1038/mtna.2013.66.
URL http://dx.doi.org/10.1038/mtna.2013.66https://linkinghub.elsevier.com/retrieve/pii/S2162253116301974

9 S. Tavakoli, O. K. Kari, T. Turunen, T. Lajunen, M. Schmitt, J. Lehtinen, F. Tasaka, P. Parkkila, J. Ndika, T. Viitala, H. Alenius, A. Urtti, A. Subrizi, Diffusion and Protein Corona Formation of Lipid-Based Nanoparticles in the Vitreous Humor: Profiling and Pharmacokinetic Considerations, Molecular Pharmaceutics 18 (2) (2021) 699–713. doi:10.1021/acs.molpharmaceut.0c00411.

10 S. F. Dowdy, Endosomal escape of RNA therapeutics: How do we solve this rate-limiting problem?, RNA 29 (4) (2023) 396–401. doi:10.1261/rna.079507.122.
URL http://rnajournal.cshlp.org/lookup/doi/10.1261/rna.079507.122

11 W. Poon, B. R. Kingston, B. Ouyang, W. Ngo, W. C. Chan, A framework for designing delivery systems, Nature Nanotechnology 15 (10) (2020) 819–829. doi:10.1038/s41565-020-0759-5.
URL http://dx.doi.org/10.1038/s41565-020-0759-5

12 W. Li, C. Wang, Y. Zhang, Y. Lu, Lipid Nanocarrier-Based mRNA Therapy: Challenges and Promise for Clinical Transformation, Small 2310531 (2024) 1–21. doi:10.1002/smll.202310531.

13 I. Bos, M. Timmerman, J. Sprakel, FRET-Based Determination of the Exchange Dynamics of Complex Coacervate Core Micelles, Macromolecules 54 (1) (2021) 398–411. doi:10.1021/acs.macromol.0c02387.

14 K. Ueda, Y. Sakagawa, T. Saito, T. Fujimoto, M. Nakamura, F. Sakuma, S. Kaneko, T. Tokumoto, K. Nishimura, J. Takeda, Y. Arai, K. Yamamoto, Y. Ikeda, K. Higashi, K. Moribe, Molecular-Level Structural Analysis of siRNA-Loaded Lipid Nanoparticles by 1H NMR Relaxometry: Impact of Lipid Composition on Their Structural Properties, Molecular Pharmaceutics (2023). doi:10.1021/acs.molpharmaceut.3c00477.

15 J. Gilbert, F. Sebastiani, M. Y. Arteta, A. Terry, A. Fornell, R. Russell, N. Mahmoudi, T. Nylander, Evolution of the structure of lipid nanoparticles for nucleic acid delivery: From in situ studies of formulation to colloidal stability, Journal of Colloid and Interface Science 660 (October 2023) (2024) 66–76. doi:10.1016/j.jcis.2023.12.165.
URL https://linkinghub.elsevier.com/retrieve/pii/S0021979723025080

16 J. Philipp, A. Dabkowska, A. Reiser, K. Frank, R. Krzysztoń, C. Brummer, B. Nickel, C. E. Blanchet, A. Sudarsan, M. Ibrahim, S. Johansson, P. Skantze, U. Skantze, S. Östman, M. Johansson, N. Henderson, K. Elvevold, B. Smedsrød, N. Schwierz, L. Lindfors, J. O. Rädler, pH-dependent structural transitions in cationic ionizable lipid mesophases are critical for lipid nanoparticle function, Proceedings of the National Academy of Sciences 120 (50) (2023) 2017. doi:10.1073/pnas.2310491120.
URL http://www.pnas.org/lookup/suppl/doi:10.1073/pnas.2216830120/-/DCSupplemental.https://doi.org/10.1073/pnas.2216830120https://pnas.org/doi/10.1073/pnas.2310491120

17 L. Adhikari, H. Mishra, M. Semalty, A. Semalty, Small Angle Neutron Scattering in Drug Discovery Research: A Novel Tool for Advanced Study of Structures of Biological Macromolecules, Current Drug Discovery Technologies 20 (5) (9 2023). doi:10.2174/1570163820666230515162614.
URL https://www.eurekaselect.com/216942/article

18 F. Sebastiani, M. Yanez Arteta, M. Lerche, L. Porcar, C. Lang, R. A. Bragg, C. S. Elmore, V. R. Krishnamurthy, R. A. Russell, T. Darwish, H. Pichler, S. Waldie, M. Moulin, M. Haertlein, V. T. Forsyth, L. Lindfors, M. Cárdenas, Apolipoprotein E Binding Drives Structural and Compositional Rearrangement of mRNA-Containing Lipid Nanoparticles, ACS Nano 15 (4) (2021) 6709–6722. doi:10.1021/acsnano.0c10064.
URL https://pubs.acs.org/doi/10.1021/acsnano.0c10064

19 G. Giubertoni, M. Bonn, S. Woutersen, D2O as an Imperfect Replacement for H2O: Problem or Opportunity for Protein Research?, The Journal of Physical Chemistry B 127 (38) (2023) 8086–8094. doi:10.1021/acs.jpcb.3c04385.
URL https://pubs.acs.org/doi/10.1021/acs.jpcb.3c04385

20 L. Willner, A. Poppe, J. Allgaier, M. Monkenbusch, D. Richter, Time-resolved SANS for the determination of unimer exchange kinetics in block copolymer micelles, Europhysics Letters (EPL) 55 (5) (2001) 667–673. doi:10.1209/epl/i2001-00467-y.
URL https://iopscience.iop.org/article/10.1209/epl/i2001-00467-y

21 I. Grillo, Applications of stopped-flow in SAXS and SANS, Current Opinion in Colloid and Interface Science 14 (6) (2009) 402–408. doi:10.1016/j.cocis.2009.04.005.

22 J. Lu, F. S. Bates, T. P. Lodge, Addition of Corona Block Homopolymer Retards Chain Exchange in Solutions of Block Copolymer Micelles, Macromolecules 49 (4) (2016) 1405–1413. doi:10.1021/acs.macromol.5b02395.

23 Y.-T. Lee, L. D. Pozzo, Contrast-Variation Time-Resolved Small-Angle Neutron Scattering Analysis of Oil-Exchange Kinetics Between Oil-in-Water Emulsions Stabilized by Anionic

Surfactants, Langmuir 35 (47) (2019) 15192–15203. doi:10.1021/acs.langmuir.9b02423.
URL https://pubs.acs.org/doi/10.1021/acs.langmuir.9b02423

24 T.-Y. Heo, S. Kim, L. Chen, A. Sokolova, S. Lee, S.-H. Choi, Molecular Exchange Kinetics in Complex Coacervate Core Micelles: Role of Associative Interaction, ACS Macro Letters 10 (9) (2021) 1138–1144. doi:10.1021/acsmacrolett.1c00482.
URL https://pubs.acs.org/doi/10.1021/acsmacrolett.1c00482

25 T. Shoaib, J. M. Ha, Y. Han, W. R. Chen, C. Do, SANS characterization of time dependent, slow molecular exchange in an SDS micellar system, Physical Chemistry Chemical Physics 24 (28) (2022) 16988–16996. doi:10.1039/d2cp00930g.

26 H. Y. Saad, W. I. Higuchi, Water Solubility of Cholesterol, Journal of Pharmaceutical Sciences 54 (8) (1965) 1205–1206. doi:10.1002/jps.2600540826.
URL https://linkinghub.elsevier.com/retrieve/pii/S0022354915350243

27 D. K. Madan, D. E. Cadwallader, Solubility of Cholesterol and Hormone Drugs in Water, Journal of Pharmaceutical Sciences 62 (9) (1973) 1567–1569. doi:10.1002/jps.2600620947.
URL https://linkinghub.elsevier.com/retrieve/pii/S0022354915412134

28 G. Settanni, W. Brill, H. Haas, F. Schmid, pH-Dependent Behavior of Ionizable Cationic Lipids in mRNA-Carrying Lipoplexes Investigated by Molecular Dynamics Simulations, Macromolecular Rapid Communications 2100683 (2021) 1–10. doi:10.1002/marc.202100683.

29 M. Hammel, Y. Fan, A. Sarode, A. E. Byrnes, N. Zang, P. Kou, K. Nagapudi, D. Leung, C. C. Hoogenraad, T. Chen, C. W. Yen, G. L. Hura, Correlating the Structure and Gene Silencing Activity of Oligonucleotide-Loaded Lipid Nanoparticles Using Small-Angle X-ray Scattering, ACS Nano 17 (12) (2023) 11454–11465. doi:10.1021/acsnano.3c01186.

30 C. Recsei, R. A. Russell, M. Cagnes, T. Darwish, Deuterated squalene and sterols from modified Saccharomyces cerevisiae, Organic & Biomolecular Chemistry 21 (32) (2023) 6537–6548. doi:10.1039/D3OB00754E.
URL https://xlink.rsc.org/?DOI=D3OB00754E

31 A. Sokolova, J. Christoforidis, A. Eltobaji, J. Barnes, F. Darmann, A. E. Whitten, L. de Campo, BILBY: Time-of-Flight Small Angle Scattering Instrument, Neutron News 27 (2) (2016) 9–13. doi:10.1080/10448632.2016.1163980.
URL https://www.tandfonline.com/doi/full/10.1080/10448632.2016.1163980

32 A. Sokolova, A. E. Whitten, L. de Campo, J. Christoforidis, A. Eltobaji, J. Barnes, F. Darmann, A. Berry, Performance and characteristics of the BILBY time-of-flight small-angle neutron scattering instrument, Journal of Applied Crystallography 52 (1) (2019) 1–12. doi:10.1107/S1600576718018009.
URL https://scripts.iucr.org/cgi-bin/paper?S1600576718018009

33 H. Yu, A. Angelova, B. Angelov, B. Dyett, L. Matthews, Y. Zhang, M. El Mohamad, X. Cai, S. Valimehr, C. J. Drummond, J. Zhai, Real-Time pH-Dependent Self-Assembly of Ionisable Lipids from COVID-19 Vaccines and In Situ Nucleic Acid Complexation, Angewandte Chemie International Edition 62 (35) (8 2023). doi:10.1002/anie.202304977.
URL https://onlinelibrary.wiley.com/doi/10.1002/anie.202304977

34 M. F. Trollmann, R. A. Böckmann, mRNA lipid nanoparticle phase transition, Biophysical Journal 121 (20) (2022) 3927–3939. doi:10.1016/j.bpj.2022.08.037.

35 J. L. Thelen, W. Leite, V. S. Urban, H. M. O'Neill, A. V. Grishaev, J. E. Curtis, S. Krueger, M. M. Castellanos, Morphological Characterization of Self-Amplifying mRNA Lipid Nanoparticles, ACS Nano 18 (2) (2024) 1464–1476. doi:10.1021/acsnano.3c08014.
URL https://pubs.acs.org/doi/10.1021/acsnano.3c08014

36 J. J. Richards, C. L. Whittle, G. Shao, L. D. Pozzo, Correlating structure and photocurrent for composite semiconducting nanoparticles with contrast variation small-Angle neutron scattering and photoconductive atomic force microscopy, ACS Nano 8 (5) (2014) 4313–4324. doi:10.1021/nn405914g.

37 M. Hibino, S.-i. Takata, K. Hiroi, H. Aoki, T. Terashima, Dynamic Exchange of Amphiphilic Random Copolymers between Micelles in Water: Kinetics and Mechanism Analyzed by TR-SANS, Macromolecules (4 2023). doi:10.1021/acs.macromol.2c02408.
URL https://pubs.acs.org/doi/10.1021/acs.macromol.2c02408

38 J. Lu, F. S. Bates, T. P. Lodge, Remarkable effect of molecular architecture on chain exchange in triblock copolymer micelles, Macromolecules 48 (8) (2015) 2667–2676. doi:10.1021/acs.macromol.5b00294.

39 Y. Gerelli, L. Porcar, L. Lombardi, G. Fragneto, Lipid exchange and flip-flop in solid supported bilayers, Langmuir 29 (41) (2013) 12762–12769. doi:10.1021/la402708u.

40 R. X. Gu, S. Baoukina, D. P. Tieleman, Cholesterol Flip-Flop in Heterogeneous Membranes, Journal of Chemical Theory and Computation 15 (3) (2019) 2064–2070. doi:10.1021/acs.jctc.8b00933.

41 M. Ramezanpour, D. P. Tieleman, Computational Insights into the Role of Cholesterol in Inverted Hexagonal Phase Stabilization and Endosomal Drug Release, Langmuir 38 (24) (2022) 7462–7471. doi:10.1021/acs.langmuir.2c00430.

42 SasView 5.0.5.
URL http://www.sasview.org/

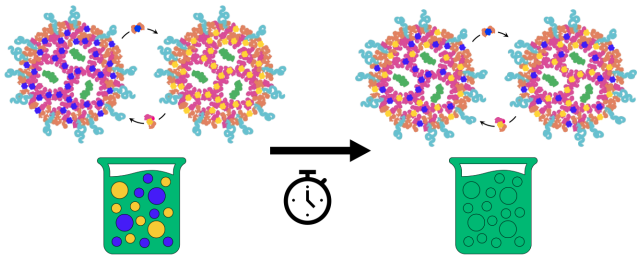

Fig. 7 Graphical Abstract